# Graphene physics and insulator-metal transition in compressed hydrogen

Ivan I. Naumov, R. E. Cohen, and Russell J. Hemley

Phys. Rev. B **88**, 045125 — Published 22 July 2013

DOI: 10.1103/PhysRevB.88.045125

# Graphene physics and insulator-metal transition in compressed hydrogen

Ivan I. Naumov, R. E. Cohen and Russell J. Hemley
*Geophysical Laboratory, Carnegie Institution of Washington,*
*5251 Broad Branch Road, Washington, D.C. 20015, USA*
(Dated: July 8, 2013)

Compressed hydrogen passes through a series of layered structures in which the layers can be viewed as distorted graphene sheets. The electronic structures of these layered structures can be understood by studying simple model systems- an ideal single hydrogen graphene sheet and three-dimensional model lattices consisting of such sheets. The energetically stable structures result from structural distortions of model graphene-based systems due to electronic instabilities towards Peierls or other distortions associated with the opening of a band gap. Two factors play crucial roles in the metallization of compressed hydrogen: (i) crossing of conduction and valence bands in hexagonal or graphene-like layers due to topology and (ii) formation of bonding states with $2p_z$ $\pi$ character.

PACS numbers: 67.63.Cd, 67.80F-, 71.30.+h

## I. INTRODUCTION

The creation and characterization of metallic hydrogen under pressure has been described by Ginzburg as one of the "Key Problems of Physics and Astrophysics"[1]. Hydrogen in a metallic state is expected to exhibit high-$T_c$ superconductivity[2] and other exotic properties, and achieving such a state is thus of great fundamental interest. At low temperatures hydrogen forms a simple hexagonal close packed structure with freely rotating molecules, called phase I[3]. At such temperatures, the material transforms to the quantum broken symmetry phase (phase II) at pressures of 125 GPa and phase III at 150 GPa[3]. The transition to phase III is characterized by a strong change in the infrared vibron absorption.

Recently, solid hydrogen has been intensively investigated in a new pressure-temperature domain (200-360 GPa, and just above 300 K), both experimentally[4–9] and theoretically[10–15]. A new phase (phase IV) has been discovered above 220 GPa in the higher temperature regime[4,5,8]. Though several different structures have been proposed for phase IV from first-principles calculations,[11,12,15] there is agreement that this phase can be viewed as a mixed– layer structure, where layers of weakly interacting $H_2$ molecules are sandwiched between graphene-like layers.

Since the band structures associated with $1s$ electrons in a hydrogenic honeycomb lattice and $2p_z$ electrons in graphene are identical both topologically and by symmetry[16], two seemingly unrelated topics in modern condensed matter physics– graphene physics and hydrogen metallization are intimately interconnected. This interconnection is wider than might appear at first sight. In fact, the stability of solid hydrogen in structures consisting of graphene-like hexagonal sheets was predicted in 1981[17], well before the discovery of graphene. Using ab-initio calculations we show that the electronic properties of *all* the proposed candidate structures for solid molecular hydrogen at high density can be understood by studying a single graphene layer and/or simple systems composed of such layers. The structures can be viewed as underlying model graphene layers that are distorted due to intrinsic electronic instabilities leading to the appearance of an excitonic insulator, Peierls distortion or molecular tilting.

This analysis leads us to identify two new factors that can control the metallization of compressed hydrogen. We show that hydrogenic hexagonal- or graphene-like layers form band states with Dirac-type cones where the bonding valence and antibonding conduction bands inevitably touch each other leading to the zero-gap semiconductor or semimetallic behavior. This effect explains why many proposed structures with nearly the same energy and symmetry exhibit nevertheless distinct band structures in the vicinity of the Fermi level $E_F$. We also show that lowering of the bonding $2p_z$ and other states comes into play above 200 GPa when the energy difference between the $1s$ and $2p$ atomic orbitals become comparable with the bandwidths of the $1\sigma_g$ and $1\sigma_u^*$ states. The implications of these results for experiments, and in particular the interpretation of recent optical data, is presented elsewhere[18]

## II. METHODS

Calculations were performed using density functional theory as implemented in the ABINIT package. A 16×16×1 Monkhorst-Pack $\boldsymbol{k}$-point grid has been used in the case of the ideal hydrogenic honeycomb lattice containing only two atoms per cell; approximately the same $\boldsymbol{k}$-point density was retained in going from the 2D honeycomb lattice to 3D systems. The sheets have been simulated by a slab-supercell approach with inter-planar distances of 25 $a_B$ to ensure negligible wavefunction overlap between the replica sheets. For the plane-wave expansion of the valence and conduction band wave functions, a cutoff energy was chosen to be 40 Ha. A norm-conserving pseudopotential with a cutoff radius of 0.5 a.u. was first generated using OPIUM codes and then used, along with the Wu-Cohen exchange and correlation functional[19]. The obtained results were tested against

all-electron FLAPW calculations, and very good consistency between the two was found.

## III. RESULTS

### A. A single honeycomb layer

We begin with a discussion of the electronic and atomic properties of a 2D honeycomb hydrogenic lattice under pressure, which we mimic by changing the nearest distance between two hydrogen atoms $b$. At zero pressure, this distance was found to be 1.177 Å, which is considerably larger than that found for a 6-membered hexagon with $D_{6h}$ symmetry (0.992 Å)[14]. This reflects the fact that chemical bonding in an isolated hexagon is stronger than in a periodic network of such hexagons, where each atom must share its electron with three neighbors.

The band structure of an ideal 2D hydrogenic honeycomb lattice is shown in Fig. 1. When the bond length $b$ is larger than 1.10 Å, this structure is similar to that in carbon graphene, where the conduction and valence bands touch each other in a linear fashion at two inequivalent Dirac points, $\mathbf{K}$ and $\mathbf{K'}$, connected by time-reversal symmetry (Fig. 1a). However, the next (and higher) energy level(s) at Γ are very sensitive to the lattice spacing and quickly move downwards as the lattice parameter decreases, as shown by a vertical arrow in Fig. 1a. As a result, at $b$ =1.10 Å, the second energy level becomes lower than the Dirac level, and the system undergoes a transition from a zero-gap semiconductor to a semimetallic state, Fig. 1b. This level is the bottom of the bonding $2p_z$ band, so that the transition is accompanied by the charge flow from the antibonding $1s$ orbitals to the bonding $2p_z$ orbitals.

The ideal honeycomb lattice is unstable with respect to structural distortions. The existence of Dirac cones implies that there are nestings between the valence and conduction bands, which can be expressed as

$$-\epsilon_i(\boldsymbol{k}) = \epsilon_j(\boldsymbol{k}) \tag{1a}$$

or

$$-\epsilon_i(\boldsymbol{k}) = \epsilon_j(\boldsymbol{k} + \boldsymbol{K} - \boldsymbol{K'}), \tag{1b}$$

where the $\boldsymbol{k}$ vector is measured relative to a Dirac point and the valence ($i$) and conduction ($j$) band energies are measured relative to $E_F$; note that the difference $\boldsymbol{K} - \boldsymbol{K'}$ is again a Dirac point plus a reciprocal lattice vector. The conditions (1a) and (1b) lead to strong electron-phonon coupling and Kohn anomalies in phonon spectra $\omega_\lambda(\boldsymbol{q})$ for vibrations with $\boldsymbol{q} = \Gamma$ or $\boldsymbol{q} = \boldsymbol{K}$. Such anomalies manifest themselves as sharp kinks and have been observed in carbon systems– graphite and bilayer graphene[20,21]. They should also exist in the hydrogenic honeycomb lattice and even be stronger in the absence of $sp^2$ bonding. Special attention must be given to the soft phonon modes with $\boldsymbol{q} = \boldsymbol{K}$ capable of opening up the gap at the Dirac points via $\boldsymbol{K} - \boldsymbol{K'}$ mixing. These modes are actually the transverse optical (TO) and longitudinal acoustic (LO) modes that have been studied in Ref.[22]. When frozen, they break the translation symmetry and lead to $\sqrt{3} \times \sqrt{3}$ superstructures which can be viewed as 2D Peierls-like distortions[23].

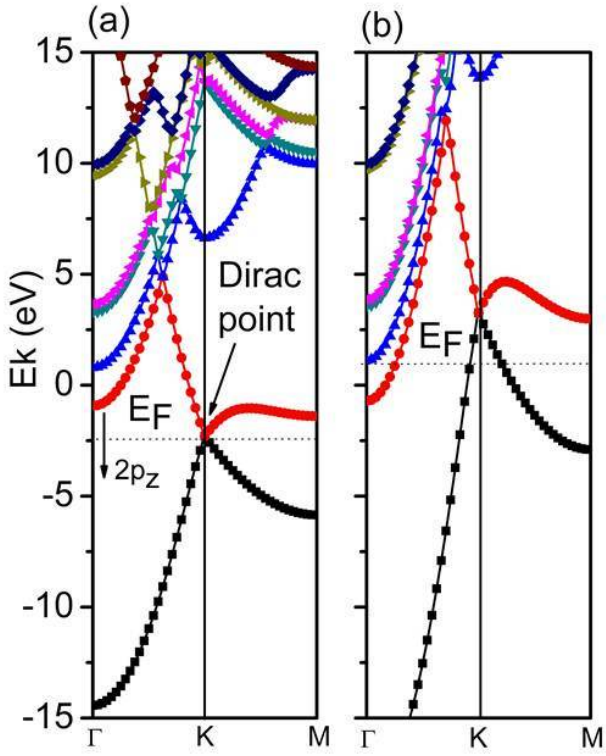


FIG. 1: (color online) Calculated band structure of H-graphene for two different bond lengths: (a) $b$=1.23 Å and (b) $b$=0.94 Å. The vertical arrow in (a) indicates the bonding conduction band $2p_z$ moving quickly downward as the lattice parameter decreases. At $b$=1.10 Å this band becomes lower than the Dirac level as seen in (b). The equilibrium $b$=1.177 Å. Note that the bands are colored in order of energy.

We now consider the stability of the lattice against such distortions for different lattice parameters. The TO (or so-called Kekulé) distortion can be introduced via in-plane atomic displacements preserving the initial $D_{6h}$ point symmetry. It can be described by only one structural parameter or amplitude, $\delta$, which can be either positive or negative (Fig. 2). Positive $\delta$'s lead to the dimerization of ab initial atomic lattice where the intramolecular distance is $b(1-\delta)$, and the intermolecular distance $b(1+\delta/2)$, where $b$ is the initial bond length. In contrast, negative $\delta$'s describe the process of breaking of the initial lattice into smaller hexagons ("hexamerization") in which the nearest distance between different hexagons is $b(1-\delta)$, whereas the bond length inside the

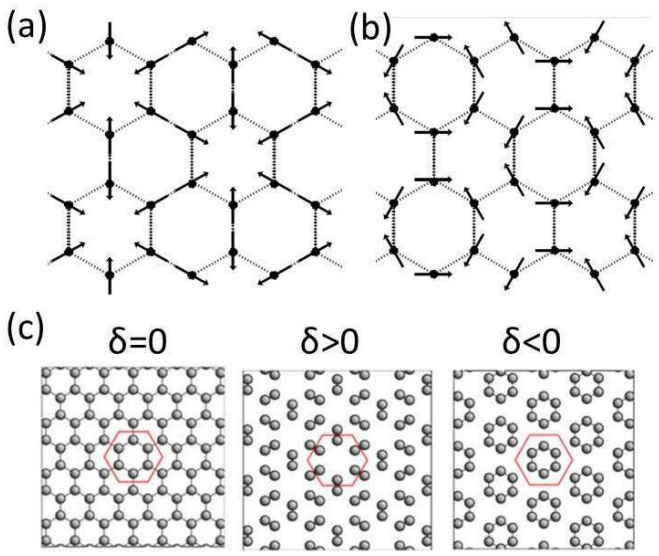


FIG. 2: (color online) Peierls distortions of a honeycomb lattice, leading to a $\sqrt{3}\times\sqrt{3}$ superstructure and described by an amplitude $\delta$. (a) TO distortion, (b) LA distortion; modified after Ref.[22]. (c) TO distortions for different $\delta$; $\delta$=0 corresponds to a pristine honeycomb lattice where a non-primitive unit cell is chosen in the form of hexagon. In the case of $\delta > 0$ the initial lattice dimerizes, so that the initial atomic hexagon expands. In the case of $\delta < 0$, the initial lattice hexamerizes, and the initial atomic hexagon decreases in size. Modified after Ref.[23].

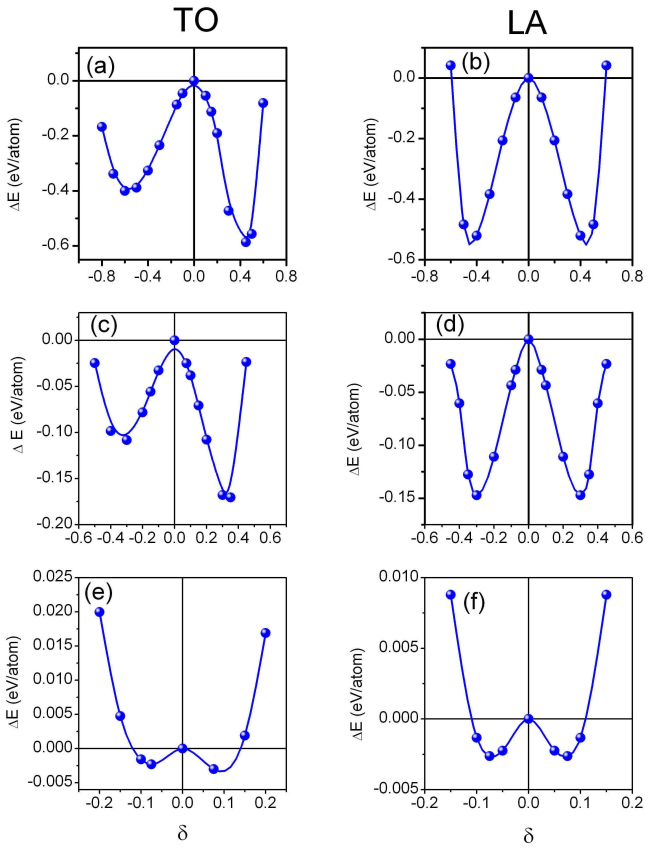


FIG. 3: (color online) Total energy vs TO and LA mode amplitude $\delta$ for different initial bond lengths $b$: (a,b) 1.40 Å, (c,d) 1.177 Å and (e,f) 1.0 Å. The TO and LA modes are actually symmetrized to produce the distortions of the $D_{6h}$ and $D_{3h}$ symmetries, respectively.

new, smaller hexagons is given by $b(1+\delta/2)$.

Similar to the TO Peierls distortions, the LA counterparts can also be described by a single amplitude $\delta$ (Fig. 2). The LA distortions reduce the symmetry from $D_{6h}$ to $D_{3h}$, and the corresponding energy profile is symmetric with respect to the change of the sign of $\delta$. Both $\delta > 0$ and $\delta < 0$ lead to the dimerization of hydrogen atoms where the resulting intramolecular and intermolecular distances are $b(1-|\delta|)$ and $b(1+|\delta|)$, respectively.

The energy profiles calculated as a function of the amplitude $\delta$ for different initial bond lengths $b$ are shown in Fig. 3. In the case of TO distortions, such profiles exhibit two asymmetric minima, one for $\delta >0$ and the other for $\delta <0$. The first one corresponding to dimerization of hydrogen atoms is more stable than the second leading to separated hexagons. This is in agreement with early results[17] showing that the energy of the hexagonal $H_6$ complex is higher than that of three $H_2$ molecules. The minimum for $\delta > 0$ is not only deeper but also sharper because here the atoms in each pair move towards each other and at some point start mutually repelling as the separation becomes somewhat less than 0.75 Å, the bond length in isolated $H_2$.

The profiles for the LA Peierls distortions are similar to that for TO counterparts with $\delta >0$; this is not surprising because in both cases they describe the process of dimerization. Again, the minima correspond to a intramolecular distance of 0.75 Å and are sharp in form due to the repulsion of the H atoms below this critical separation. Figure 3 shows that the wells become progressively shallower and closer to each other as the initial bond length is decreased. Just below $b = 1$ Å, the minima merge and the energy profile becomes single-welled. This point correlates well with the moment when the bonding $2p_z$-band at Γ passes the Dirac energy (1.1.Å). This fact can be easily understood. The Peierls distortions mix the unperturbed $\boldsymbol{K}$ and $\boldsymbol{K'}$ Bloch states and break the 4-fold degeneracy at Γ of a pristine honeycomb lattice into two 2-fold degeneracies, opening the gap and lowering the total energy. But the latter can happen only when the Dirac point coincides with the Fermi level. The is not the case when the $2p_z$ band near Γ becomes noticeably lower than the Fermi level, thus eliminating the driving force for the Peierls distortions. Though freezing of these modes opens up a gap at Dirac points and lowers the total energy, it does not effect much the pace of the lowering of the $2p_z$ states.

Analysis shows that the ideal honecomb lattice can be unstable against other distortions leading to the dimer-

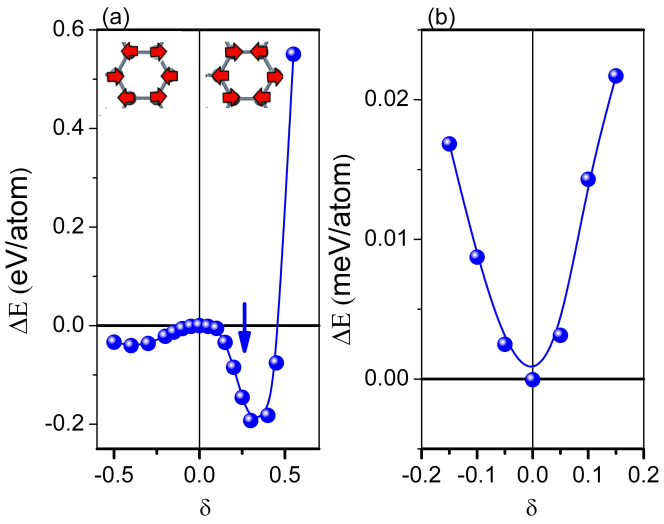


FIG. 4: (color online) Total energy vs Γ optical phonon amplitude $\delta$ for different initial bond lengths $b$: (a) 1.177 Å and (b) 1.0 Å. The inserts illustrate that in case of $\delta > 0$ two nearest hydrogen atoms in each unit cell approach each other, whereas for $\delta < 0$ they move away from each other. The vertical blue arrow indicates the moment when two Dirac points merge to open a band gap.

ization of hydrogen atoms. These distortions, however, become energetically less favorable than the Peierls type for the initial bond lengths $b$ shorter than $\sim 1.15$ Å. To illustrate this, consider, for example, the simplest path for the association of hydrogen atoms into molecules when two nearest hydrogen atoms in each unit cell move towards each other. The distortion can be visualized as a freezing of the optical phonon mode at the Γ point. As for the TO($\boldsymbol{K}$) and LA($\boldsymbol{K}$) symmetrized modes, this distortion can be described by a single parameter $\delta > 0$ defining the distance between the initially nearest atoms, $b(1-\delta)$ (see inset in Fig. 4a). For comparison, we will also consider the case $\delta < 0$ when the atoms move apart so that the initial hexagonal lattice transforms toward a rectangular lattice corresponding to $\delta = -0.5$. The energy as a function of $\delta$ is shown in Fig. 4; it is similar to that for TO($\boldsymbol{K}$) distortions. At $b$=1.177 Å it exhibits two highly assymmetric minima, for positive and negative $\delta$. The first one, associated with the pairing of the hydrogen atoms, is significantly deeper. It is even slightly deeper than the minima for the Peierls distortions corresponding to the same initial $b$ (Fig. 3c,d). However, as seen from Fig. 4b, for $b$=1.0 Å, double well profile is already turned into single-welled, in contrast with the profiles in Fig. 3e,f. This proves that the Peierls distortions energetically are the most preferable distortions for the relartively short initial bond lengths $b$. Note that in the case of $\delta < 0$ for $b$=1.177 Å, the minimum forms just before the structure becomes rectangular. This minimum is very shallow because the intramolecular distance on this path can not be smaller than $b\sqrt{3}/2 \sim 1.02$ Å and the molecules with the optimal bond length $\sim 0.75$ Å cannot form.

A closer examination of Fig. 4 reveals that the position of the minimum in panel (a) for $\delta > 0$ is very close to the bond length in an isolated $H_2$ molecule, 0.75 Å. Before this minimum is reached, the energy curve exhibits the steepest fall exactly at the moment when two Dirac points shifted from their initial positions merge at the point $(\boldsymbol{G}_1 - \boldsymbol{G}_2)/2$, where $\boldsymbol{G}_1$ and $\boldsymbol{G}_2$ are the two shortest reciprocal lattice vectors forming the angles $60^0$ and $-60^0$ with the line connecting two nearest atoms separated by the distance $b(1-\delta)$. This suggests that opening a gap is one of the major stabilizing factors in compressed hydrogen.

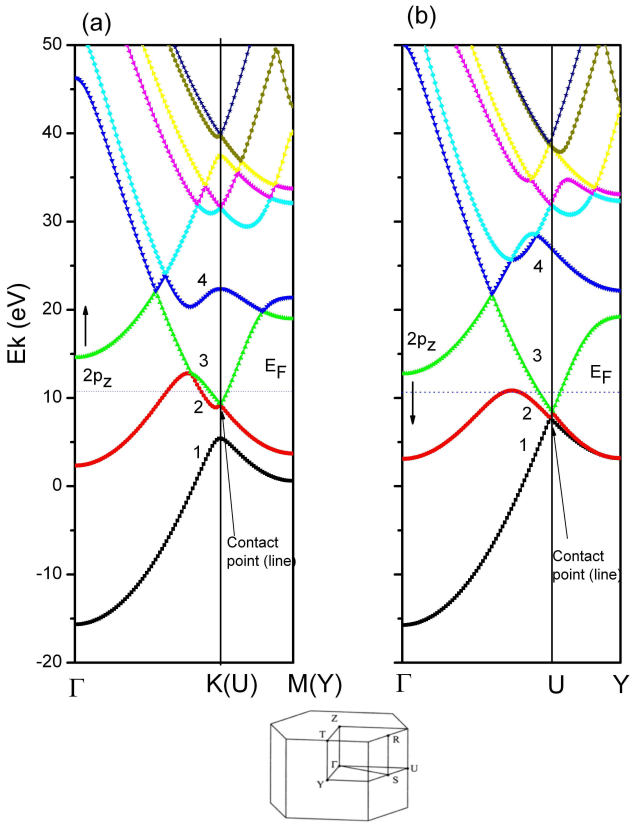


FIG. 5: (color online) Calculated band structures at 260 GPa: (a) for $P6_3/mmc$ and (b) for $Cmca$-4. For the sake of comparison, the high symmetry points in the hexagonal Brillouin zone of the $P6_3/mmc$ structure are indicated by double labels with the orthorhombic labels in parentheses.

We point out that the states with Peierls distortions can be equally interpreted as excitonic insulators characterized by charge-density oscillations, as discussed by Halperin and Rice[24]. Indeed, condition (1) also means that the electron and hole Fermi surfaces are identical in size and shape–a necessary condition for the formation of the excitonic insulators. Another necessary condition– weak screening of Coulomb interactions between electrons and holes– is also fulfilled in hydrogen graphene

due the vanishing density of states at the Dirac points and the single-atom thickness of the system. Therefore, excitonic states are likely to form in compressed hydrogen, especially at low temperatures.

The (Peierls) distortions considered above are not the only ones capable of inducing an energy gap at the Fermi level in a 2D honeycomb hydrogenic lattice via $\boldsymbol{K}$ and $\boldsymbol{K'}$ mixing. Other distortions with non-zero wavevectors can also do this, provided that their amplitude exceeds some (usually small) critical value[25]. Among such Peierls-like distortions are the $3 \times 2$ superstructures in which the length of the super-period along zigzag type directions are larger than that in honeycomb lattice by a factor of 3, whereas the super-period along an armchair type direction is larger by a factor of 2.

### B. Stacked honeycomb layers

We now consider 2D hydrogen honeycomb lattices stacked in AB (Bernal[26]) fashion to produce a 3D graphite hexagonal structure with $P6_3/mmc$ symmetry. In the 3D lattice there are four atoms per unit cell, twice as many in the honeycomb layer. Each layer must give rise to two three-dimensional states near the $\boldsymbol{K}$ and $\boldsymbol{K'}$ points of the hexagonal Brillouin zone. So the four initial single-layer bands mix together by interlayer interactions in order to form the band structure in the vicinity of $\boldsymbol{K}$ and $\boldsymbol{K'}$ points[27]. Though the AB stacking destroys the sublattice or inversion symmetry in each single layer, the necessary condition for the formation of Dirac degeneracy points, such points nevertheless do survive in the 3D structure due to the interlayer interactions[27], as seen from Fig. 5a. Moreover, the degeneracy points merge together along the vertical edges HKH of the hexagonal Brillouin zone, thus forming band-contact lines. These lines exhibit the following interesting topological property: the line integral of the Berry connection for any curve enclosing them is $\pm\pi$[29].

In Fig. 5a we present the band structure for this $P6_3/mmc$ structure calculated at a pressure of 260 GPa. We indicate the energy bands in the vicinity $\boldsymbol{K}$ and $\boldsymbol{K'}$ points by by 1, 2, 3 and 4 in order to stress that they originate from the mixing of the initial layer states. It is remarkable that their forms are in qualitative agreement with that predicted in Ref.[27] for carbon graphite on the basis of tight-binding calculations. From Fig. 5a it is clearly seen that at $\boldsymbol{K}$, the 2-fold degenerate state lies between the two single levels, thus forcing the valence and conduction bands to touch[27]. Since band 2 exhibits a local maximum near the $\boldsymbol{K}$ point, the Fermi level is forced also to cross band 3 as well. As a result, in contrast to the 2D hydrogen honeycomb lattice, this system represents a semimetal without involving of the $2p_z$ states.

The bonding $2p_z$ states in the $P6_3/mmc$ structure fall at the bottom of the third band near $\Gamma$, Fig. 5a. At P=0, their energies practically coincide with the Fermi level $E_F$ but gradually move away from the latter as the lattice parameter is decreased. As a result, at 260 GPa, they become well above the $E_F$, by 3 eV. This is not the case, for example, in the *Cmca*-4 phase, as we will see below. We stress that the degenerate states on the contact-band lines (HKH) in the $P6_3/mmc$ structure transform according to a two dimensional representation and the lines themselves coincide with the 3-fold symmetry lines. However, due to their topological properties, these contact lines are stable against any (not too severe) lattice distortions including those breaking 3-fold symmetry. As a result the contact-band lines may shift from the high-symmetry lines in the Brillouin zone becoming curved in shape like spirals. (Such a spiral ending up on the faces of the Brillouin zone is found, for example, in the rhombohedral graphite with ABC stacking[26,28].)

### C. Analysis of candidate structures

Though a graphene motif is most evident in the candidate structures *Cc, Pc* and *Pbcn* for phase IV[11–14], it can be also found in other candidate structures proposed for dense hydrogen. Thus, the distorted hexagons are clearly seen in the layered $C2/c$ and *Cmca*-4 structures. The former is the most plausible candidate for the low temperature phase III and the latter is a predicted at higher pressures and low temperatures[7,11,12]. The intermolecular distance in graphene-like layeres of high-pressure structures like $C2/c$,*Cc, Pc* and *Pbcn* is on the order of 1.0–1.1 Å[11–14]. This is noticeably shorter than the minimal distance separating two hydrogen atoms from the neighboring layers (1.4 –1.5 Å). We expect therefore that such layers play a key role in forming their electronic properties and atomic structures.

Among these candidate structures, the $C2/c$ phase would appear to be a very large distortion of an ideal honeycomb lattice. Yet such a comparison is possible. To mimic this phase we designed an artificial phase where four ideal honeycomb layers are the stacked equidistantly in a ABCD fashion in such a way that resulting symmetry is again $C2/c$. In fact, this model structure can be continuously transformed within the given symmetry into the phase $C2/c$ by moving the atoms inside the unit cell. As seen from the Fig. 6, the band structure of the model system does mimic well that of $C2/c$, especially above and below the Fermi level. The main difference, of course, is in the vicinity of $E_F$ where the model structure exhibits, in contrast to $C2/c$, an overlap of the conduction and valence bands producing a metal. Such a difference is not surprising because each layer in the $C2/c$ structure can be considered as a $\sqrt{3} \times \sqrt{3}$ superstructure relative to an ideal graphene sheet; in this superstructure the initial graphene $\boldsymbol{K}$ and $\boldsymbol{K'}$states are mixed to form a band gap. Hence, according to Sec. A, this structure can be viewed as a Peierls or excitonic insulator phase.

We find that the band structures of all the other candidate phases can be understood in this way, including

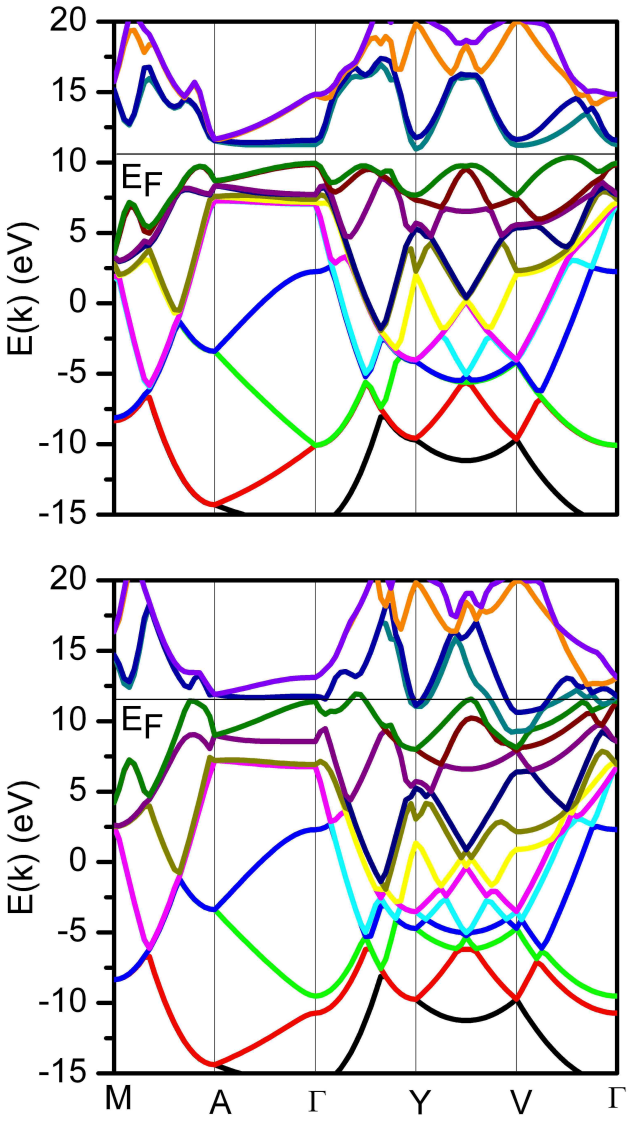


FIG. 6: (color online) The band structures of the $C2/c$ phase at 300 GPa (a) and of an artificial phase composed from four ideal honeycomb layers ABCD in such a way that the resulting symmetry is also C2/c (b). The artificial phase, like $C2/c$, has 24 atoms per cell and its lattice parameters are also identical to that for the $C2/c$ structure. The notation of the symmetrical points is borrowed from Ref.[11]

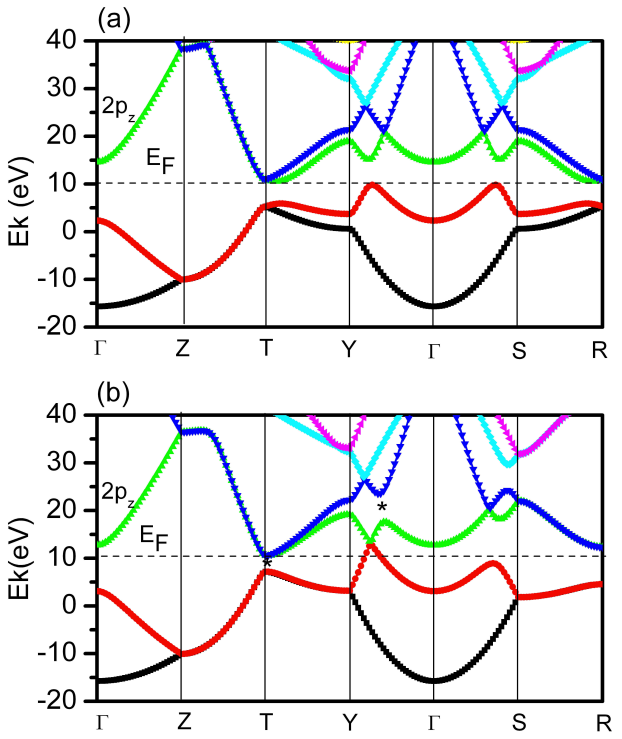


FIG. 7: (color online) Same as in Fig. 5, but for other directions in the orthorhombic Brillouin zone. In panel (b), the star * indicates the band gaps that appear due to molecular tilting, $\theta \neq 0$.

mixed phases like *Cc, Pc* and *Pbcn*[11–14], where the layers of unbound $H_2$ molecules are sandwiched between the graphene-like layers. The situation with *Pbcn* structure, for example, is similar to that for $C2/c$. Here again the insulating behavior of the systems can be easily explained: each layer in the *Pbcn* structure can be presented as a $3\times2$ superlattice stabilized by Peierls-like distortions that mix the Dirac states $\boldsymbol{K}$ and $\boldsymbol{K'}$ and open an energy gap (see Sec. A).

Let us consider in more detail the *Cmca*-4 structure, which geometrically is close to the hydrogen graphite structure with space group $P6_3/mmc$ discussed in Sec. B. Like the $P6_3/mmc$ structure, it can also be considered as a layered structure with ABAB stacking where the $H_2$ molecules form an angle $\theta \sim 30^0$ with respect to the $xy$ plane. As seen from Fig. 5 (b) this structure, like $P6_3/mmc$, exhibits band-contact lines which now coincide well with the vertical lines passing through the U points. The character of splitting of energy levels at the U point is different from that at the $\boldsymbol{K}$ and $\boldsymbol{K'}$ points in $P6_3/mmc$ structure: the degeneracy point lies below the single levels. Another difference is that now the $1s$ orbitals associated with band 4 near the U point are strongly hybrydized with bonding $2p_z$ orbitals. It is the hybridization that makes the $2p_z$ orbitals behave differently in the comparable systems as the pressure increases. We found that at 260 GPa the $2p_z$ level at Γ in the *Cmca*-4 phase is 4 eV above the $E_F$. However, the former moves quickly down with pressure and passes the $E_F$ at $\sim$ 300 GPa. But even before this critical pressure the system is already in a semimetallic state due shifting of the $E_F$ relative to the contact point (Fig. 5b).

As the above analysis shows, the hybridization is due to the orientational tilting of hydrogen molecules enabling mixing of $1s$ and $2p_z$ orbitals to form $sp$ like orbitals. This tilting opens up a gap at the Fermi level at the T

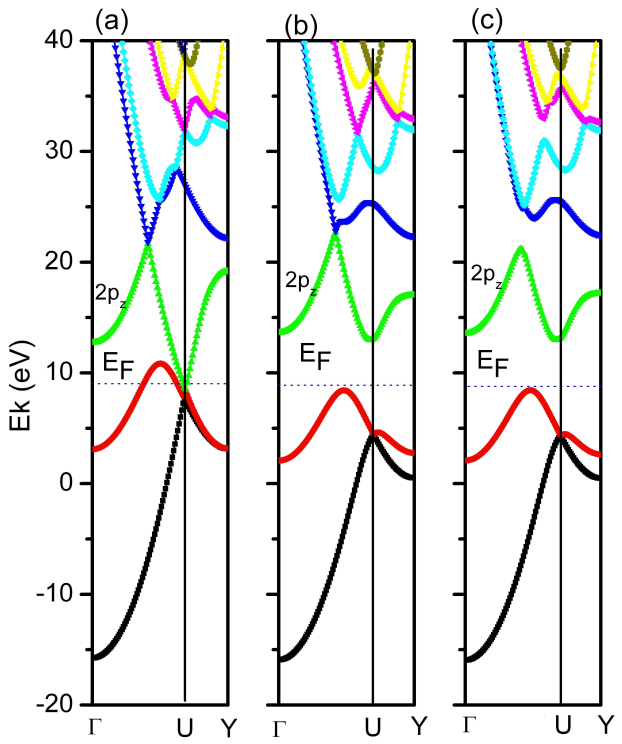


FIG. 8: (color online) Calculated band structures: (a) for *Cmca*-4 at 260 GPa, (b) for $Cmc2_1$, and (c) for $C2/m$ phases. In going from *Cmca*-4 to $Cmc2_1$ the lattice parameters, intramolecular distances and tilting angles are kept the same. The only difference between these structures is that in the latter the centers of molecules lie almost on an ideal hcp lattice. The $C2/m$ structure differs from $Cmc2_1$ only by mutual orientation of two molecules in the unit cell, whereas in the it $Cmc2_1$ structure the molecular axes are tilted by the angles $\theta$ and $-\theta$ from the $xy$ plane, in the $C2/m$ the axes are parallel, i.e. molecules tilted by the same angle, $\theta \sim 30^0$.

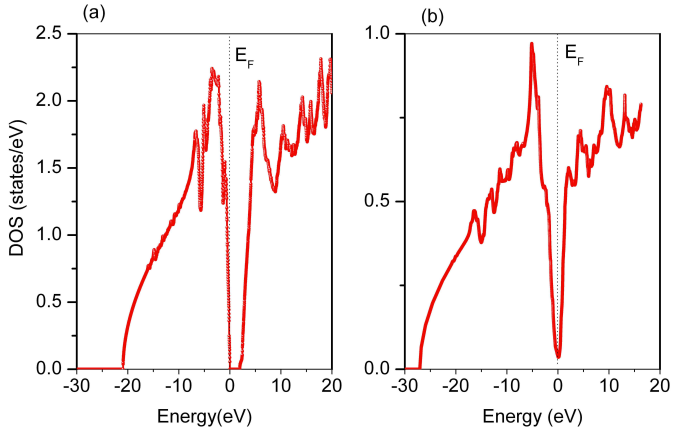


FIG. 9: (color online) Density of states (DOS) : (a) for $C2/m$ at 150 GPa and (b) for *Cmca*-4 at 300 GPa. The calculations have been performed by using the tetrahedron method and sufficiently dense k-point meshs: 40×40×40 and 100×100×8 for the $C2/c$ and *Cmca*-4 structures respectfully.

point, as shown in Fig. 7b. The rotation of hydrogen molecules tends to prevent the the system from being (semi)metallic. Despite this fact the valence and conduction bands cross each other near the U points due to topological reasons, as in Fig. 5b .

This crossing, however, can be easily destroyed by sliding of alternate layers of towards the polar $Cmc2_1$ structure, as shown in Fig. 8b. The reason is that such a sliding breaks an effective in-plane inversion symmetry-the center of symmetry of a 2D lattice obtained by projection of two nearest layers on the $xy$ plane. The energy gap at the U point also opens up in the $C2/m$ structure where such a symmetry center is also broken, as in Fig. 8c. Though the opening of a gap due to a *Cmca*-4 to $Cmc2_1$ structural transformation has already been discussed in the literature (e.g., Ref.[30]), the physical reason for this was not clear.

## IV. DISCUSSION

Our results suggest two possible mechanisms for the metallization of compressed hydrogen. The first one is related to the fact that in the systems with honeycomb-structured or graphene-like layers a metallic electronic structure occurs because of symmetry and topology, as, for example, in graphite-structured hydrogen or the *Cmca*-4 phase. The first metallization mechanism involves only 1$s$ bands, whereas the second mechanism involves 1s valence states and $2p_z$ conduction states. Under pressure, the bonding $2\pi$ states associated with the atomic $2p_z$ orbitals become lower in energy than the antibonding $1\sigma_u^\star$ states originating from the 1$s$ orbitals. The fact that the $2p_z$ bands come into play at elevated pressures is not surprising –the energy difference between the 1$s$ and 2$p$ atomic orbitals becomes comparable with the widths of the $1\sigma_g$ and $1\sigma_u^\star$ bands (∼10 eV). The decrease in the band gap due to these two effects can (and usually does) widen again due to Peierls-like distortions or molecular tilting; this delays the transition to higher pressures at low temperatures.

In accordance with these two mechanisms, we found that metallization in all the candidate structures occurs over only a very small fraction of the Brillouin zone when small pieces of Fermi surface first form (see also[33,34]). As a result, the density of states (DOS) at the Fermi level remains relatively low not only just after the system enters a metallic state but also for higher pressures. In *Cmca*-4, for example, N(E$_F$) ∼ 0.05 states/eV at 300 GPa, i.e. approximately 200 GPa above the gap closure (Fig. 9b). Surpisingly, the general form of the DOS does not change much in passing from one structure to another, as seen by comparing the Figures 9a and 9b. This partly explains why the main features of the optical properties of

different candidate structures are similar[18].

As a potential high-$T_c$ superconductor, dense hydrogen in some respects is similar to $MgB_2$. The latter is also a layered material where boron atoms form a hexagonal lattice consisting of honeycomb layers stacked in AA fashion; and its band structure[35] is similar, for example, to that of *Cmca*-4. Like $MgB_2$, compressed hydrogen should not belong to the conventional superconductors requiring a high desity of states at $E_F$. But similar to $MgB_2$, it can have strong electron-phonon coupling (and therefore be a high temperature superconductor) due to the quasi-two dimensionality of the electronic structure[36], quite strong covalent bonding[37] and high phonon frequencies[38].

Despite the similarities, there are fundamental differences between H-graphene and C-graphene. The two have a similar electronic structure and represent a zero-gap insulator with topologically protected Dirac points at $\boldsymbol{K}$ and $\boldsymbol{K'}$. However, in C-graphene the $sp^2$ states provide most of the structural stability and completely suppress the Peierls instability associated solely with the $2p_z$ states. In H-graphene, the relationship between the electronic and atomic structures is more subtle, because the same $1s$-electrons provide the bonding and structural stability. As a result, ideal H-graphene sheets find a variety of different ways to open a band gap at the Dirac points and reduce the total energy. Among the most effective distortions are the Peierls (or Peierls-like) distortions that induce the energy gap via $\boldsymbol{K}$ and $\boldsymbol{K'}$ mixing. These displacements lead to the formation of superlattices that are multiples of 3 or $\sqrt{3}$ from the primitive graphene cell; such superlattices indeed were found in the proposed phases for dense hydrogen(e.g., *Pbcn, Cc, C2/c*). The systems also avoid the crossing of 1s and $2p_z$ bands by mixing them, as in the case of diamond-type Si where the mixing of $3s$ and $3p$ bands form a gap along the Γ-X direction[32]. To enable the $1s - 2p_z$ mixing in a graphene layer, the $H_2$ pairs should tilt out of the ideal honeycomb plane. Such a tilting was found, for example, in the molecular layers of the *Pbcn* structure and in all layers of the $C2/c$ structure.

In summary, we have shown that compressed hydrogen can reach a semimetallic state via (i) the formation of bits of Fermi surface representing the intersections of Dirac cones from graphene related structures (near the $\boldsymbol{K}$-point in ideal graphene) or (ii) closing of an indirect band gap between the valence and conduction bands originating principally from $1s$ and $2p_z$ atomic orbitals, respectively. A consideration of quantum and thermal fluctuations should not change our conclusions. These fluctuations will serve to broaden the band states and initiate band overlap at lower compressions than indicated here, as shown in[31]. However, the discontinuity in the potential at $E_F$ or electron self-interaction will increase the gap. These two effects of opposite sign will at least partly cancel, as discussed in Ref.[10]. In any event, the graphene-like layers will dominate the behavior of high pressure hydrogen, its metallization, and other optical and electronic properties.

## V. ACKNOWLEDGEMENTS

We thank N. W. Ashcroft, I. I. Mazin, C. S. Zha and S. Mandal for helpful discussions and are grateful to S. A. Gramsch for comments on the manuscript. This research was supported by EFree, an Energy Frontier Research Center funded by the U.S. Department of Energy, Office of Science, Basic Energy Sciences under Award DE-SC0001057. The infrastructure and facilities used are supported by U.S. National Science Foundation (DMR-1106132) and the U.S. Department of Energy/National Nuclear Security Administration (DE-FC-52-08NA28554, CDAC).

[1] V. L. Ginzburg, Phys. Usp. **42**, 353 (1999).
[2] N. W. Ashcroft, Phys. Rev. Lett. **21**, 1748 (1968).
[3] H. K. Mao and R. J. Hemley, Rev. Mod. Phys. **66**, 671 (1994).
[4] M. I. Eremets and I. A. Troyan, Nature Materials, **10**, 927 (2011).
[5] R. T. Howie, C. L. Guillaume, T. Scheler, A. F. Goncharov, and E. Gregoryanz, Phys. Rev. Lett., **108**, 125501 (2012).
[6] C. S. Zha, Z. Liu, and R. J. Hemley, Phys. Rev. Lett., **108**, 146402 (2012).
[7] A. F. Goncharov, J. S. Tse, H. Wang, J. Yang, V. V. Struzhkin, R. T. Howie, and E. Gregoryanz, Phys. Rev. B **87**, 024101 (2013).
[8] C. S. Zha, Z. Liu, M. Ahart, R. Boehler, and R. J. Hemley, Phys. Rev. Lett., **110**, 217402 (2013).
[9] P. Loubeyre, F. Occelli, and P. Dumas, Phys. Rev. B **87**, 134101 (2013).
[10] C. J. Pickard and R. J. Needs, Nature Physics **3**, 473 (2007).
[11] C. J. Pickard, M. Martinez-Canales, and R. J. Needs, Phys. Rev. B **85**, 214114 (2012); Phys. Rev. B **86**, 059902(E) (2012).
[12] H. Liu, L. Zhu, W. Cui and Y. Ma, J. Chem. Phys. **137**, 074501 (2012).
[13] V. Labet, P. Gonzalez-Morelos, R. Hoffmann, and N. W. Ashcroft, J. Chem. Phys. **136**, 074501 (2012).
[14] V. Labet, R. Hoffmann, and N. W. Ashcroft, J. Chem. Phys. **136**, 074502 (2012); **136**, 074503 (2012); **136**, 074504 (2012).
[15] H. Liu and Y. Ma, Phys. Rev. Lett. **110**, 025903 (2013).
[16] R. Saito, G. Dresselhaus, and M. S. Dresselhaus, *Physical Properties of Carbon Nanotubes* (Imperial College, London, 1998).
[17] R. LeSar and D. R. Herschbach, J. Phys. Chem. **85**, 3787 (1981).
[18] R. E. Cohen, Ivan I. Naumov, and Russell J. Hemley, PNAS, in press.
[19] Z. Wu and R. E. Cohen, Phys. Rev. B **73**, 235116 (2006).
[20] S. Piscanec, M. Lazzeri, F. Mauri, A.C. Ferrari, and J. Robertson, Phys. Rev. Lett. **93**, 185503 (2004).
[21] D. L. Mafra, L. M. Malard, S. K. Doorn, H. Htoon, J. Nilsson, A. H. Castro Neto, and M. A. Pimenta, Phys. Rev. B **80**, 241414(R) ( 2009).
[22] D. Gunlycke, H. M. Lawler, and C. T. White, Phys. Rev. B **75**, 085418 (2007).
[23] S. M. Lee, H. J. Chung, J. Heo, H. Yang, H. J. Shin, U. I. Chung, and S. Seo, ACS NANO **5**, 2964 (2011).
[24] B. I. Halperin and T. M. Rice, Rev. Mod. Phys. **40**, 755 (1968).
[25] I. I. Naumov and A. M. Bratkovsky, Phys. Rev. B **85**, 201414(R) (2012).
[26] J. C. Charlier, X Gonze, and J. P. Michenaud, Carbon **32**, 289 (1994).
[27] J. C. Slonczewski and P. R. Weiss, Phys. Rev. **109**, 272 (1958).
[28] J. W. McClure, Carbon **7**, 425 (1969).
[29] G. P. Miktik and Yu. V. Sharlai, Phys. Rev. Lett. **82**, 2147 (1999).
[30] J. B. Neaton, and N. W. Ashcroft, Nature **400**, 141 (1999).
[31] A. M. Morales, J. M. McMahon, C. Pierleoni, and D. M. Ceperley, http://arxiv.org/abs/1303.6673 (2013).
[32] A. K. McMahan, Physica B and C, **139** and **140B**, 31 (1986).
[33] I. I. Mazin and R. E. Cohen, Phys. Rev. B **52**, R8597 (1995).
[34] P. Cudazzo, G. Profeta, A. Sanna, A. Floris, A. Continenza, S. Massidda, and E. K. U. Gross Phys. Rev. B **81**, 134505 (2010).
[35] J. Kortus, I. I. Mazin, K. D. Belashchenko, V. P. Antropov, and L. L. Boyer, Phys. Rev. Lett., **86**, 4656 (2001).
[36] W. E. Pickett , J. M. An, H. Rosner, and S.Y. Savrasov, Physica C **387** 117 (2003).
[37] H. J. Choi, D. Roundy, H. Sun, M. L. Cohen, and S. G. Louie, Nature, **418**, 756 (2002).
[38] P. Cudazzo, G. Profeta, A. Sanna, A. Floris, A. Continenza, S. Massidda, and E. K. U. Gross, Phys. Rev. B **100**, 257001 (2008).